




Degradation of agricultural pollutants by biopolymer-enhanced photocatalysis: application of Taguchi method for optimization

Rogelio Estrada-Vázquez¹ · Mabel Vaca-Mier² · Victoria Bustos-Terrones³ · Jesús Gabriel Rangel-Peraza¹ · Juan G. Loaiza¹ · Jhonatan J. Hermosillo-Nevárez⁴ · Yaneth A. Bustos-Terrones⁵ 

Received: 24 August 2023 / Accepted: 30 September 2023 / Published online: 19 October 2023
© Akadémiai Kiadó, Budapest, Hungary 2023

Abstract

This paper evaluates the photocatalytic degradation of malathion using titanium dioxide (TiO₂) nanoparticles supported on sodium alginate (SA), polyvinyl alcohol (PVA), polyvinyl pyrrolidone (PVP) polymer beads and ultraviolet light as irradiation source with a wavelength of 254 nm. Six different types of beads were prepared: SA, PVA, PVP, SA/TiO₂, PVA/TiO₂, and PVP/TiO₂ to assess the effect of the adsorbent material on the photodegradation process by optimizing an experimental design using the Taguchi method. Four factors were considered: TiO₂ concentration, bead mass, polymer type, and initial malathion concentration. The response variables were the percentage of removal of the contaminant and the removal rate calculated from the first-order kinetic models. A malathion degradation of 99% was achieved after 180 min of operation when using 100 g and 200 g of SA/TiO₂, PVA/TiO₂, and PVP/TiO₂ beads. The best operating conditions were 1 g L⁻¹ of TiO₂, 100 g of bead mass, SA polymer, and 5 mg L⁻¹ of malathion initial concentration. This study found that the adsorption process affected negatively the photodegradation process, reducing the removal efficiency and rate. Finally, the feasibility of the use of a biopolymer-enhanced photocatalytic treatment to degrade agro-industrial contaminants was demonstrated.

Keywords Photocatalysis · TiO₂/UV · Malathion · Taguchi L9 · Biopolymers

Introduction

In recent years, the agricultural industry has shown accelerated growth worldwide due to the different intensive techniques applied and different uses of agrochemicals and pesticides [1]. Organophosphorus compounds are the most used due to their high effectiveness in pest control [2]. However, due to their chemical stability,

Extended author information available on the last page of the article

resistance to biodegradation, and high solubility in water, they are easily transported to surface and underground water bodies and terrestrial ecosystems through precipitation, irrigation, infiltration, erosion, and runoff [3].

The contamination of water resources by agricultural residues has become more important in recent years, due to its high toxicity and adverse effects on human health [4, 5], becoming a concern worldwide [6]. The current study focuses on the elimination of malathion, which is a highly used organophosphate pesticide, which is widely present in agricultural effluents and waterbodies, particularly in regions with high agricultural activity [7]. Malathion concentrations between 3.3 and 5 mg L⁻¹ can cause cytotoxicity to cells of the human central nervous system [3]. Hepatotoxic effects have also been reported in marine species [8] and rats [9]. Despite this situation, agricultural effluents are treated through conventional techniques, such as physical and biological processes. These processes are inefficient in removing non-biodegradable and chemically stable contaminants from contaminated effluents [10, 11].

To reduce these impacts, photocatalysis emerged as a technologically viable, sustainable, and novel alternative in wastewater treatment [12–14], due to its main advantages such as its ability to degrade recalcitrant pollutants, and the oxidation of organic compounds to CO₂ and water. In addition, the catalysts commonly used in this process, such as TiO₂ and ZnO, are innocuous and can be reused [15–18]. ZnO has been widely used as a catalyst in the photodegradation of various pollutants. Farzadkia et al. [19], evaluated the photodegradation efficiency of metronidazole in an aqueous solution. They reported a maximum photodegradation of 96.55% of metronidazole and 95.42% of COD by optimizing the pH, UV irradiation time, irradiation power, and nano-ZnO load in a hydraulic retention time of 3 h. Likewise, Rodriguez-Mata et al. [20] evaluated the photo degradation of the 2, 4-dichlorophenoxyacetic acid pesticide, when implementing ZnO and SO₂⁻⁴/ZnO as catalysts. They obtained a removal efficiency of 38.4% when using ZnO and 82.3% with the doped catalyst (SO₂⁻⁴/ZnO) in a hydraulic retention time of 6 h, showing that photocatalysis is an alternative for mitigation of pollution problems from agricultural activities.

Recently, some studies have opted for the use of TiO₂ in the photocatalysis process due to its high photocatalytic activity, large surface area, low cost, non-toxicity, and excellent stability under lighting [21–24]. Juang and Chen et al. [6], compared the photodegradation of two agricultural pollutants, Methomyl and Parathion, when using TiO₂ particles as catalyst and UV light as irradiation source. Both compounds were completely degraded in 90 and 120 min of operation. Kadam et al. [25] evaluated the photocatalytic activity of nitrogen-doped titanium dioxide (N/TiO₂) nanostructures in malathion degradation. They studied the effect of pH, catalyst load, and irradiation sources. Under the best process conditions (pH 6; 1 g dm⁻³ of N/TiO₂ and 150 min of UV light irradiation), they observed a maximum degradation of 97% of malathion. Besides, they demonstrated that the by-products resulting from the process were less toxic than malathion. Surendra et al. [10] studied the effect of malathion photocatalytic degradation as a function of contact time by using Ni/TiO₂ nanoparticles. They observed a maximum removal of 94% of malathion in 80 min. Akter et al. [26] investigated the photodegradation of sulfamethoxazole (SMX),

metronidazole (MNZ), and ciprofloxacin (CIP) by commercial TiO_2 in a reactor with a 254 nm ultraviolet lamp as the irradiation source. They obtained a maximum removal efficiency of 97% of SMX in 360 min of operation with 5 mg L^{-1} of initial concentration of the pollutant, 100% of MNZ in 600 min with an initial concentration of 80 mg L^{-1} , and 89% of CIP in 600 min. with an initial concentration of 80 mg L^{-1} . The dose of the catalyst used in the process was 0.7 g L^{-1} . Finally, they concluded that the use of TiO_2 with UV radiation is a promising process for the efficient treatment of pharmaceutical wastewater. However, when using the catalyst in the form of nanoparticles, the catalyst recovery from the treated water is difficult and requires the use of various subsequent techniques, increasing the costs of the process.

To solve this inconvenience, some studies recommend the use of a support for the catalyst. Commonly, this support can be calcium alginate, sodium alginate, palm fiber, and polyvinyl alcohol [5, 24, 27–29]. The use of these polymers eases the separation of the catalyst after the photocatalysis process and could be reused [15, 30–36]. However, there are few studies where the photocatalysis process is conducted using supports since it is a complex process where the adsorption and photodegradation phenomena occur simultaneously. These works have so far omitted the effect of the adsorption process on the photocatalysis process. The present study aims to describe the behavior of the adsorption–photocatalysis processes to figure out the effect of the adsorbent material on the photodegradation of a highly persistent pollutant such as malathion. Different supports were evaluated to perform a statistical comparison of the photodegradation efficiencies and their degradation and adsorption kinetics. The best treatment efficiency was obtained using the Taguchi statistical method. In addition, the present study contributes to the mathematical modeling of the photocatalysis process and the adsorption process.

Materials and methods

Materials

All the reagents used in the work were of reagent-grade quality. Titanium isopropoxide ($\text{C}_{12}\text{H}_{28}\text{O}_4\text{Ti}$) brand Aldrich Chemistry, 97% purity. Hydrochloric Acid (HCl) Meyer brand, 38% purity. Ethanol ($\text{C}_2\text{H}_5\text{OH}$) Meyer brand, purity 99.5%. Distilled water (H_2O). Malathion ($\text{C}_{10}\text{H}_{19}\text{O}_6\text{PS}_2$) Velsimex 1000-E brand, 87.8% purity. Sodium alginate ($\text{C}_6\text{H}_7\text{O}_6\text{Na}$)n, Alquimia Brand. Polyvinyl alcohol ($\text{C}_2\text{H}_4\text{O}$)n, Alquimia brand. Polyvinyl pyrrolidone ($\text{C}_6\text{H}_9\text{NO}$)n Alquimia brand. Calcium chloride (CaCl_2), Faga Lab. brand, 96% purity.

TiO_2 synthesis

Titanium dioxide (TiO_2) nanoparticles were obtained by the Sol–Gel synthesis method [37]. Initially, 15 mL of ethanol ($\text{C}_2\text{H}_5\text{OH}$) was poured into a beaker and then 7.4 mL of titanium isopropoxide ($\text{C}_{12}\text{H}_{28}\text{O}_4\text{Ti}$) was added. The solution was

kept under constant stirring and then 10 mL of distilled water (H_2O) was added drop by drop until the solution was homogeneous. Stirring was continued for 10 min. Subsequently, 0.5 mL of hydrochloric acid (HCl) [0.1 M] was added. The system was heated to 70 °C until the excess water evaporated. Finally, a heat treatment was conducted in a muffle (Felisa) for 2 h at 500 °C. The catalyst obtained was TiO_2 in the anatase phase (Fig. S1). Fig. S1 shows the X-ray patterns recorded in the 2θ range between 10° and 100°, exhibiting an anatase phase at the diffraction peak $2\theta = 25^\circ$ [38, 39]. The presence of TiO_2 in the anatase phase is consistent with the diffraction pattern obtained in the X-ray diffractometer equipped with a copper objective of $\lambda = 1.54184 \text{ \AA}$.

TiO_2 support in sodium alginate, polyvinyl alcohol, and polyvinyl pyrrolidone beads

TiO_2 nanoparticles were supported on sodium alginate (SA), polyvinyl alcohol (PVA) and polyvinyl pyrrolidone (PVP) polymer beads. The method used was a modification to the proposal of Bustos-Terrones et al. [40], and Basu et al. [41] (Fig. 1). Three different solutions were prepared. The first solution was 2.5 (w v^{-1}) sodium alginate, adding 12.5 g of SA to 500 mL of distilled water with constant stirring at room temperature. The second solution was 2.5 (w v^{-1}) polyvinyl alcohol, adding 12.5 g of PVA to 500 mL of distilled water with constant stirring at 80 °C. The third solution was 4% (w v^{-1}) of polyvinyl pyrrolidone, adding 20 g of PVP in 500 mL of distilled water with constant stirring at 80 °C. Subsequently, the catalyst nanoparticles (TiO_2) with a concentration of 1 g L^{-1} were added to each solution. To homogenize the catalyst, magnetic stirring (HP-3100) and radiofrequency (Brason 5800) were alternated for 30 min. Then, the homogeneous mixtures were transferred drop by drop to a 2.5 w v^{-1} calcium chloride (CaCl_2) solution with a peristaltic pump (INTLLAB) to form small beads. Finally, the beads were kept in the CaCl_2 solution for 24 h to reinforce their solidification.

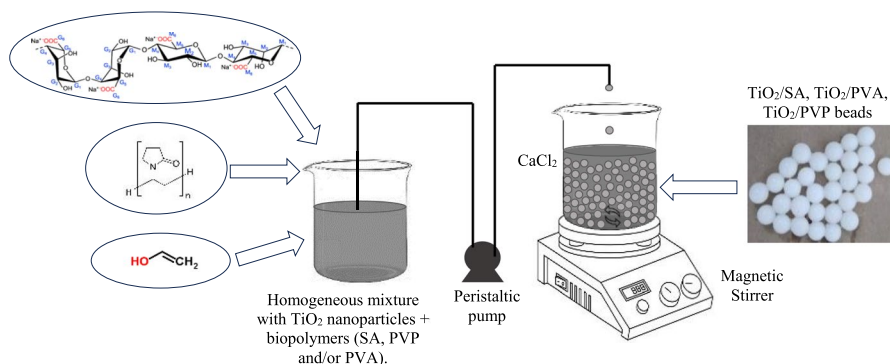


Fig. 1 Preparation scheme for SA, PVA, and PVP beads supported with TiO_2 nanoparticles. TiO_2 concentration = 1 g L^{-1} ; 2.5 w v^{-1} of SA; 2.5 w v^{-1} of PVA; 4 w v^{-1} of PVP; 2.5 w v^{-1} of CaCl_2

Characterization of SA/TiO₂, PVA/TiO₂ and PVP/TiO₂ beads

SA/TiO₂, PVA/TiO₂, and PVP/TiO₂ beads were characterized by Scanning Electron Microscopy (SEM). The characterization study of the beads was conducted before and after the photocatalysis process to make a morphological and surface comparison of them. In addition, the size of the polymer beads was measured using a Vernier caliper.

Evaluation of adsorption and photocatalytic activity

The photocatalytic activity in the degradation of malathion was evaluated using TiO₂ in suspension and TiO₂ supported on polymer beads (SA, PVA, and PVP) in a batch-type glass reactor (13 cm in diameter and 15 cm in height) with a volume capacity of 1 L (Fig. S2). The reactor was on a stirring plate (HP-3100), allowing the fluidization of the sample. Inside, it featured a quartz lamp irradiating UV light with a wavelength of 254 nm. The photodegradation process was studied using a UV–Vis spectrophotometer (Hach DR6000). The absorbance wavelength for this contaminant was 330 nm. Preliminary tests were carried out to determine the detection limits of the spectrophotometer. These tests involved preparing a series of standard solutions with known concentrations of malathion and measuring their absorbance. The calibration curve was used to determine the detection limit by identifying the concentration at which the signal-to-noise ratio (S/N) reached a 10:1 value [42]. Based on these tests, synthetic samples of agricultural wastewater were prepared with malathion in a concentration of 6 mg L⁻¹. Subsequently, the photocatalysis process was evaluated with different masses of beads (50, 100, and 200 g) of the polymers with catalyst (SA/TiO₂, PVA/TiO₂, and PVP/TiO₂), beads without catalyst (SA, PVA, and PVP) and TiO₂ in suspension. Samples of 7 mL were taken every 15 min for around 3 h during malathion degradation. Samples in All experiments were performed at room temperature (25 °C). The removal efficiency was calculated using Eq. (1) [43].

$$\%R = \left(\frac{c_0 - c_e}{c_0} \right) \times 100 \quad (1)$$

Here % R = Removal efficiency, (%); C₀ = initial concentration, (mg L⁻¹); C_e = steady state concentration, (mg L⁻¹).

Mathematical modeling

Three different processes for the elimination of malathion were evaluated: adsorption, direct photocatalysis, and the effect of adsorption–photocatalysis. First, the malathion adsorption process with the different support polymers was evaluated independently. This process was conducted with a hydraulic retention time of 1 h. In parallel, the malathion photodegradation process was evaluated without the

influence of the adsorption process. UV light was irradiated right at the start of the process (time=0) to ensure that the photocatalysis takes place at once without the adsorption process influencing the removal of malathion. The hydraulic retention time of the photocatalysis process was 3 h. In addition, the adsorption–photocatalysis process was evaluated. In this process, the adsorption process took place for 60 min. After this time, the system was irradiated with UV light for 3 h to start the photocatalysis process and identify if the contaminant adsorbed on the surface interferes with the malathion photodegradation process. Therefore, the hydraulic retention time of the adsorption–photocatalysis process was 4 h. These processes were described mathematically using the equations given below.

Adsorption kinetics

The adsorption kinetics by Lagergren's pseudo-first-order model was evaluated in this study using Eq. (2) [21, 44].

$$q_t = q_e * (1 - e^{-k_1 t}) \quad (2)$$

Here q_e = amount of malathion at equilibrium per unit mass of adsorbent, (mg g^{-1}); q_t = amount of malathion adsorbed per unit mass of adsorbent at time t , (mg g^{-1}); k_1 = pseudo-first-order rate constant, (min^{-1}). This mathematical model predicts malathion pesticide adsorption through time.

First-order photodegradation kinetics

The data obtained through the malathion photodegradation process were fitted to the first-order exponential model. The kinetics of photodegradation was described following the following equation [45]:

$$C_t = C_0 * e^{-kt} \quad (3)$$

Here: C = malathion concentration, (mg L^{-1}); k = is the first order constant, (min^{-1}). This mathematical model predicts the photodegradation of the pesticide malathion through time.

Adsorption isotherms

The Langmuir and Freundlich isotherms were studied because they are adsorption models adopted to study the distribution of malathion in an aqueous solution through the adsorbent phase [5, 21, 27, 43, 46]. Equation (4) describes the Langmuir isotherm model used and the Freundlich isotherm model used corresponds to Eq. (5).

$$q_e = \frac{q_{max} K_L C_e}{1 + K_L C_e} \quad (4)$$

$$q_e = K_F C_e^{1/n} \quad (5)$$

Here: q_e = Amount of adsorption per unit mass of adsorbent in equilibrium, (mg g^{-1}); C_e = equilibrium concentration of the pollutant in the solution, (mg L^{-1}); q_{max} = adsorption capacity per unit mass of adsorbent, (mg g^{-1}); K_L = Langmuir's constant based on the affinity of the adsorbate binding site per adsorbent (L g^{-1}). By plotting the experimental data of adsorption capacity (q_e) against the equilibrium concentration (C_e) and fitting the data to the Langmuir isotherm equation, the values of q_{max} and K_L were obtained; K_F and n = Freundlich constants that are related to adsorption capacity and adsorption intensity.

Experimental design

The study of the malathion photodegradation process was conducted using a Taguchi L9 orthogonal array. The Taguchi method reduces the number of executions of experiments using orthogonal matrices and has been applied in different areas to establish parameters of interest [36, 47]. According to Suresh et al. [48], biopolymer-based photocatalysis is influenced by some crucial operating variables, such as biopolymer composition and mass, the wavelength and energy of light source, irradiation time, catalyst type and concentration, temperature, pH and the initial concentration of the pollutant. In this investigation, the study variables were the TiO_2 concentration, the number of beads, the type of polymer, and the initial concentration of malathion. These variables have been often used to optimize the photodegradation process using biopolymers, leading to more efficient and effective degradation of targeted compounds [48]. The design matrix shows the experiments carried out in the L9 orthogonal arrangement and the operating levels for each of the control variables (Table 1).

Table 1 Experimental conditions for the L9 Taguchi design

Treatment	Factor A [TiO_2]	Factor B Pearl mass (g)	Factor C Polymer	Factor D [Malathion]
1	0.5	0	SA	5
2	0.5	50	PVA	10
3	0.5	100	PVP	15
4	1	0	PVA	15
5	1	50	PVP	5
6	1	100	SA	10
7	1.5	0	PVP	10
8	1.5	50	SA	15
9	1.5	100	PVA	5

Statistical analysis

The treatments were conducted through 9 experimental runs according to the Taguchi orthogonal arrangement. In addition, 3 replicates were performed to evaluate the adsorption process, the photodegradation process, and the adsorption–photo degradation process. The statistical analysis was performed using the removal efficiency and the removal rate as response variables. An analysis of variance (ANOVA) was carried out to compare the different processes in the removal of malathion. The software used for statistical analysis was Statgraphics.

Results and discussion

Characterization of polymer beads

The morphology of the polymer bead surface with TiO_2 nanoparticles supported was studied through scanning electron microscope (SEM) before and after treatment to identify their structure (Fig. S3). The surface of SA/ TiO_2 , PVA/ TiO_2 , and PVP/ TiO_2 beads showed irregular and rough shapes, with the presence of micropores that allow the adequate and diffusive transport of contaminants present in wastewater [49]. The mean size of SA/ TiO_2 , PVA/ TiO_2 , and PVP/ TiO_2 beads was 3.27 μm . SEM images detected the presence of malathion in the micropores of the polymers, represented by the white spots of the images, which is characteristic of malathion when it is in contact with water. Likewise, TiO_2 was successfully supported on the SA, PVA, and PVP polymer beads. According to SEM results, the catalyst adheres to the beads to remain suspended, preventing them from settling into the bottom of the reactor.

Photocatalytic activity of TiO_2 in suspension

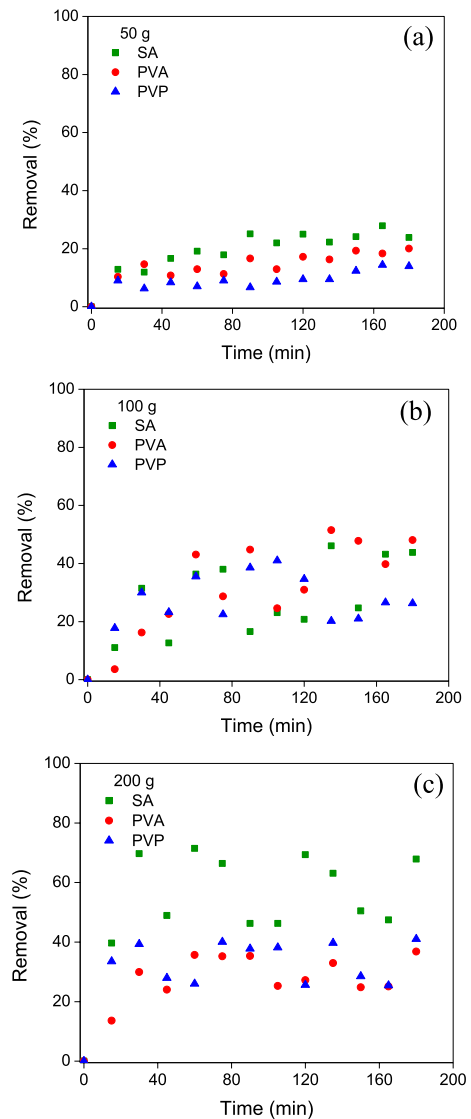
The photodegradation efficiency of the catalyst (TiO_2) in suspension was evaluated to figure out its ability to photodegrade malathion. The initial concentration of the pollutant was 6 mg L^{-1} and the hydraulic retention time was 180 min. A maximum photodegradation of 75% was obtained in 180 min of treatment (Fig. S4). In addition, the experimental data was adjusted to a first-order linear kinetic model, which shows that the mean photodegradation rate of TiO_2 in suspension is 0.068 min^{-1} , with a coefficient of determination (R^2) of 0.9553. These results are like those reported by Kumar et al. [50], who evaluated the photodegradation of organophosphate pesticides (dichlorvos and malathion) by graphene oxide- TiO_2 nanocomposites under ultraviolet radiation. They obtained 80% degradation of dichlorvos and 90% degradation of malathion in 80 min of treatment, for an initial pesticide concentration of 0.5 mg L^{-1} .

Polymer adsorption efficiency

The adsorption capacity of malathion was studied using different polymers (SA, PVA, and PVP) for 180 min. Different polymer masses were evaluated: 50, 100, and 200 g. The behavior of the adsorption process for each of the treatments with different masses of beads of all the polymers is presented in Fig. 2. This Fig. shows the percentage of malathion removed by adsorption through time.

The adsorption of the contaminant when using 50 g of polymer beads with a hydraulic retention time of 3 h is shown in Fig. 2a. Under this condition, the

Fig. 2 Malathion adsorption efficiencies by different masses (g) of SA, PVA, and PVP polymer beads versus time; a) 50 g, b) 100 g and c) 200 g of beads. Initial malathion concentration = 6 mg L⁻¹; contact time = 180 min; room temperature = 25 °C



removal efficiencies were similar for the different polymers used; however, sodium alginate resulted in the highest efficiency with a removal percentage of 30% after 160 min of treatment. Polyvinyl alcohol (PVA) achieved a maximum removal of 20% in 180 min of treatment, while polyvinyl pyrrolidone (PVP) adsorbed 15% of malathion after 180 min of treatment.

When using 100 g of beads in the treatments, the adsorption efficiencies doubled, obtaining almost a removal efficiency of 50% for the SA and PVA polymers (Fig. 2b). In the case of the PVP polymer, the highest efficiency obtained was close to 30%. In this case, an unsteady variation occurred during the process, which could be attributed to the adsorption–desorption of the pollutant. This variation could be associated with the saturation of the polymer beads and their later desorption and coincides with reports by Chakhtouna et al. [44], who suggest that adsorption occurs spontaneously at the beginning due to the high availability of sites or pores in the surface of the material. The adsorbent material reaches the largest adsorption, but the desorption process takes place immediately because the pollutant molecules find it difficult to occupy the vacant pores due to the barrier between them, generating repulsive forces between the adsorbate and the adsorbent.

Fig. 2c shows the behavior of the removal efficiency of malathion through time using 200 g of polymer beads. An increase in the adsorption efficiency was noticed, where the SA was the one that presented the highest removal average efficiency, 67.86%, ($p < 0.05$). In the case of PVA and PVP, a similar trend was observed in both treatments, with a maximum efficiency of 40%. The adsorption–desorption processes are depicted in Fig. 2c. These results are like those by Han et al. [21], who reported a maximum removal of 98.4% of methylene blue using polyacrylonitrile (PAN) beads, coated with polyvinyl alcohol (PVA) with encapsulation of TiO_2 nanoparticles.

Photocatalytic activity of SA/ TiO_2 , PVA/ TiO_2 and PVP/ TiO_2

Table 2 and Fig. S5 show a comparison of the malathion photodegradation process when the catalyst (TiO_2) was supported on polymer beads (SA, PVA, and PVP). The results showed the removal efficiencies through time by varying the mass of beads used in the treatments. The maximum efficiency using 50 g of beads was achieved with SA polymer, with a removal close to 90% during a hydraulic retention time of 180 min. The catalyst supported on PVA and PVP beads allowed removals below 53% during 180 min of treatment.

When a mass of 100 g of bead was used, a similar trend was observed for the different polymer beads since the same removal efficiencies (100%) in 180 min of treatment were achieved. No significant difference ($p > 0.05$) was found when using 100 g and 200 g of bead. The behavior of malathion degradation through time was similar to the one observed using 100 g of bead and a maximum malathion degradation (100%) was reached after 180 min of treatment.

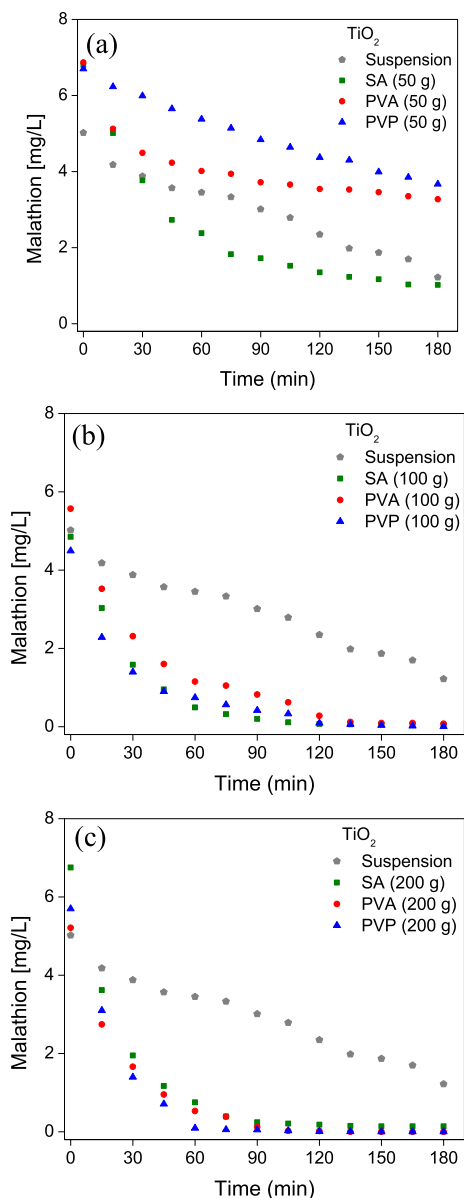
Table 2 Malathion removal by TiO₂/SA, TiO₂/PVA and TiO₂/PVP using different masses of beads (polymers)

Time (min)	50 g			100 g			200 g		
	TiO ₂ /SA	TiO ₂ /PVA	TiO ₂ /PVP	TiO ₂ /SA	TiO ₂ /PVA	TiO ₂ /PVP	TiO ₂ /SA	TiO ₂ /PVA	TiO ₂ /PVP
	0	0	0	0	0	0	0	0	0
15	27.07 ± 2.39	25.42 ± 2.38	9.31 ± 2.92	37.52 ± 3.52	36.80 ± 4.38	49.17 ± 3.62	46.37 ± 2.75	47.40 ± 3.24	45.61 ± 2.69
30	45.12 ± 3.46	34.64 ± 1.32	12.80 ± 3.46	59.17 ± 4.2	58.52 ± 3.79	68.90 ± 2.91	71.11 ± 2.89	68.13 ± 3.87	75.47 ± 3.45
45	60.26 ± 3.18	38.42 ± 1.67	17.75 ± 2.67	80.41 ± 3.74	71.27 ± 2.47	79.97 ± 2.87	82.66 ± 3.46	81.76 ± 2.49	87.56 ± 2.99
60	65.35 ± 2.63	41.57 ± 2.89	21.68 ± 2.98	89.85 ± 2.79	79.35 ± 2.58	83.51 ± 3.16	88.88 ± 2.28	89.82 ± 2.35	98.35 ± 1.62
75	73.36 ± 1.72	42.64 ± 1.25	25.18 ± 2.34	90.92 ± 1.03	81.14 ± 2.32	87.45 ± 2.94	94.22 ± 2.53	92.59 ± 2.14	99.03 ± 0.53
90	74.96 ± 1.84	45.86 ± 2.06	29.54 ± 1.47	94.84 ± 2.35	85.27 ± 3.36	90.69 ± 2.57	96.44 ± 1.97	97.57 ± 2.41	99.10 ± 0.56
105	77.87 ± 2.23	46.76 ± 1.12	32.45 ± 1.88	99.57 ± 0.42	88.86 ± 2.66	92.67 ± 1.24	96.88 ± 0.78	99.59 ± 0.26	99.49 ± 0.38
120	80.34 ± 2.07	48.47 ± 0.98	36.39 ± 1.23	99.76 ± 0.14	94.97 ± 1.34	97.98 ± 1.06	97.33 ± 0.39	99.65 ± 0.18	99.81 ± 0.13
135	82.09 ± 1.47	48.69 ± 1.03	37.40 ± 1.16	98.96 ± 0.09	97.84 ± 1.05	98.67 ± 0.72	97.77 ± 0.96	99.96 ± 0.02	99.91 ± 0.05
150	82.96 ± 1.28	49.69 ± 0.89	41.92 ± 2.25	98.35 ± 0.17	98.33 ± 0.14	99.21 ± 0.04	97.92 ± 0.87	99.97 ± 0.02	99.97 ± 0.01
165	85 ± 1.09	51.23 ± 1.24	43.95 ± 1.72	97.31 ± 0.18	98.36 ± 0.23	99.58 ± 0.16	97.92 ± 0.73	99.97 ± 0.02	99.97 ± 0.01
180	85.15 ± 1.32	52.40 ± 1.18	46.57 ± 2.13	99.93 ± 0.04	98.64 ± 0.17	99.86 ± 0.08	97.92 ± 0.91	99.97 ± 0.02	99.97 ± 0.02

Comparison of the photocatalytic activity of TiO_2 in suspension and supported TiO_2

Fig. 3 shows the comparison of the photocatalysis treatments when the catalyst (TiO_2) was used in suspension and supported on polymer beads (TiO_2/SA , TiO_2/PVA , and TiO_2/PVP). Fig. 3a shows the photocatalytic degradation of malathion when using 50 g of beads for each polymer. Greater efficiency was obtained using

Fig. 3 Comparison of malathion photodegradation process through TiO_2 nanoparticles in suspension and TiO_2 nanoparticles supported on different masses of polymer beads: a) 50 g, b) 100 g and c) 200 g of beads. Initial conditions: Contact time = 180 min; room temperature = 25 °C



TiO₂ supported on SA beads than the photocatalysis treatment with the catalyst in suspension during 180 min of treatment, even though the concentration of TiO₂ in suspension used was 1 g L⁻¹. The malathion degradation efficiency obtained was lower when the PVA and PVP beads were used. The degradation efficiencies were lower than the efficiency obtained with the SA beads and the catalyst in suspension. Fig. 3b demonstrates that the photocatalytic degradation was improved when a larger amount of bead mass (100 g) was used. Malathion degradation efficiencies above 99% were achieved after 120 min of the process. The degradation efficiencies were higher than the photocatalysis degradation using the catalyst in suspension since this treatment achieved only a 75% removal efficiency after 180 min.

Fig. 3c shows that despite increasing the mass of the polymer beads, similar efficiencies were obtained than those shown in Fig. 3b. However, the removal efficiencies obtained by using 200 g of beads showed efficiencies above 99% after 90 min of treatment. These results suggested higher degradation rates when using a larger amount of polymer mass. These results are like those reported by Mehmood et al. [18], who studied the photodegradation of triclosan and diclofenac using TiO₂ supported on poly-sulfone beads. In the first five min of treatment, they identified a rapid photodegradation of the contaminants, obtaining a degradation efficiency of 60% for diclofenac and 87% for triclosan. The removal rates doubled for both contaminants, needing only 120 min and 40 min of treatment. Table 3 summarizes the most relevant photocatalysis studies with TiO₂ supported in different matrices, including the present study.

Statistical analysis

A Taguchi L9 design was used to determine the optimum operating conditions of the biopolymer-based photocatalysis. The study factors in this research were TiO₂ concentration, pearl mass, type of polymer, and initial concentration of malathion. Each of the factors had three levels of operation. Two response variables were used: the removal rate and efficiency of malathion. The adsorption and photocatalysis processes were evaluated separately, and then the effect of biopolymer adsorption on the photocatalysis process was also assessed. The experimental times varied according to the process: the adsorption process was evaluated for 60 min, while the photocatalysis process lasted 180 min. Finally, the biopolymer-based photocatalysis was evaluated for 240 min (60 min for adsorption and 180 min for photocatalysis). Table 4 shows the results of the removal coefficient rates and efficiencies obtained through the experiments of each process.

According to the data shown in Table 4, low adsorption rates were observed for the treatments that used initial malathion concentration of 10 mg L⁻¹ and 15 mg L⁻¹. This may be because the adsorbent material was quickly saturated when exposed to high concentrations of the pesticide. This situation affected the removal adsorption rates. Adsorption efficiencies of up to 20% were achieved when an initial malathion concentration of 5 mg L⁻¹ was used (treatments 5 and 9).

The photocatalysis process was then evaluated independently, avoiding the influence of the adsorption process on the removal of malathion. In this process,

Table 3 Comparison of different photocatalysis processes with TiO₂ supported in different matrices

Catalyst	Contaminant removed	Irradiation	Removal (%)	Time (min)	References
Au/Pt/TiO ₂ nanotube film	Malathion	UV Light	98.2%	240	Yu et al. [52]
TiO ₂ /CaAlg beads	Tartrazine dry	UV light	89%	180	Dalponde et al. [30]
TiO ₂ biofilms	Microbiology wastewater	UV light	79% TOC	840	Fernández et al. [54]
TiO ₂ biofilms	<i>E. Coli</i>	UV light	–	60	Alrousan et al. [55]
Alg/TiO ₂ beads	Cr (VI)	UV light	5 PPM	15	Athanasekou et al., [56]
PSF/Alg/TiO ₂ beads	Methylene blue (MB), triclosan (TCS) and diclofenac (DCF)	UV light	99%	50, 40 and 120	Mehmood et al. [18]
TiO ₂ /CaAlg	Basic Blue 41	Sunlight	96%	180	Nouri et al. [28]
SA/TiO ₂	Malathion	UV light	99.99%	180	This work
PVA/TiO ₂	Malathion	UV light	99.99%	180	This work
PVP/TiO ₂	Malathion	UV light	99.99%	180	This work

Table 4 Results of the Taguchi L9 factorial design for removal rate and efficiency

Treatment	Factors			Adsorption			Photocatalysis			Adsorption–photocatalysis			
	A	B	C	D	Removal (%)	R ²	k (min ⁻¹)	Removal (%)	R ²	k (min ⁻¹)	Removal (%)	R ²	k (min ⁻¹)
1	0.5	0	SA	5	12.40±1.05	0.9301	0.0198	83.85±7.56	0.9736	0.009	65.91±6.43	0.9045	0.005
2	0.5	50	PVA	10	8.12±0.71	0.1037	0.0076	77.19±6.82	0.985	0.008	57.54±5.66	0.9074	0.004
3	0.5	100	PVP	15	6.69±0.58	0.15	0.02	21.75±2.09	0.8519	0.001	18.80±1.72	0.6696	0.0006
4	1	0	PVA	15	2.92±0.18	0.4542	0.0247	23.94±2.18	0.7239	0.002	2.47±0.19	0.0219	0.00009
5	1	50	PVP	5	20.32±1.89	0.4376	0.0139	77.24±5.76	0.9045	0.01	81.27±6.12	0.9203	0.009
6	1	10	SA	10	5.57±0.44	0.7959	0.0135	87.26±5.48	0.9795	0.011	74.11±5.49	0.9354	0.007
7	1.5	0	PVP	10	10.42±0.98	0.2918	0.017	70.38±6.92	0.9401	0.007	22.60±2.11	0.8047	0.001
8	1.5	50	SA	15	5.22±0.47	0.3466	0.0557	13.41±1.29	0.8931	0.0009	5.80±0.58	0.2333	0.0002
9	1.5	100	PVA	5	22.51±2.19	0.4633	0.0085	93.78±4.83	0.9783	0.013	95.03±3.27	0.9112	0.011

it was observed that the concentrations decreased significantly over time, obtaining a maximum removal efficiency of 93.78% in 180 min of operation (treatment 9). In the adsorption/photocatalysis process, no synergistic effect was found as it was expected. If a comparison is carried out between the photocatalysis and adsorption/photocatalysis processes, it can be observed that the malathion degradation efficiency decreased within the treatments. For instance, a mean removal efficiency of 83.85% was obtained in treatment 1 when the photocatalysis was used solely, and a mean removal efficiency of 65.91% was observed in the same treatment when using the adsorption/photocatalysis process. This situation can be observed in several treatments of the Taguchi L9 design.

Fig. 4 shows the experimental data fit to the first-order exponential model. Fig. 4a shows the adsorption kinetics. The adsorption rate constant (k) varied between 0.0076 and 0.0557 min^{-1} . Treatment 8 showed the highest malathion adsorption rate, with a value of $k=0.0557 \text{ min}^{-1}$. This value is higher than the one reported by Hermosillo-Nevarez et al. [7], who found a maximum adsorption rate of 0.0347 min^{-1} for malathion adsorption using recycled PVC polymers. Fig. 4b shows that treatments 1, 2, 6, and 9 adjusted well to the first-order exponential model ($r^2 > 0.95$). The degradation rate constant (k) varied from 0.0009 to 0.013 min^{-1} . The treatments that presented the highest photodegradation rates were 6 and 9, with values of $k=0.011 \text{ min}^{-1}$ and $k=0.013 \text{ min}^{-1}$. In Fig. 4c the adsorption/photocatalysis treatments 1, 2, 5, 6, and 9 showed a good degree of fit to the first-order exponential model ($r^2 > 0.90$). The degradation rate (k) was lower than the photocatalysis process solely, with a range of 0.00009 min^{-1} to 0.011 min^{-1} . The treatments with the highest malathion photodegradation rates were 5 and 9, with values of $k=0.009 \text{ min}^{-1}$ and $k=0.011 \text{ min}^{-1}$. These values are higher than those reported by Rodriguez-Mata et al. [20], who found a value of $k=0.0051 \text{ min}^{-1}$ for the photodegradation of the pesticide 2, 4-D and Fazal et al. [43], who reported a value of $k=0.0050 \text{ min}^{-1}$ for the photodegradation of methylene blue.

Li et al. [2] achieved a removal efficiency of 90% of malathion with an initial concentration of 15 μM through a photocatalysis treatment with a retention time of 30 min. The removal efficiencies reported by Li et al. [2] are like those obtained in this study, however, the malathion concentrations were lower. Kralj et al. [51] reported a malathion removal efficiency of about 90% and a degradation rate of 0.083 min^{-1} with a photocatalytic process with TiO_2 . Surendra et al. [8] achieved a removal efficiency of 95% for malathion degradation by optimizing a Box–Behnken response surface experimental design. The optimum operational conditions were pH 10, temperature = 70 $^\circ\text{C}$, a degradation time of 60 min, and a weight ratio of 1.5% Ni/ TiO_2 /volume. Yu et al. [52] reported removal efficiencies of 96% and a degradation rate of 0.0058 min^{-1} for the removal of malathion using TiO_2 as a catalyst during 240 min of photocatalysis.

Likewise, treatment 9 showed the highest removal efficiencies in the different processes: 93.78% for photocatalysis and 95.03% for adsorption/photocatalysis. The highest rates also occurred in treatment 9, where $k=0.0127 \text{ min}^{-1}$ and $k=0.0111 \text{ min}^{-1}$ were obtained for the photocatalysis and adsorption–photocatalysis processes, respectively. On the contrary, treatment 8 presented the lowest removal efficiencies in the different processes: 13.41% for photocatalysis and 5.80%

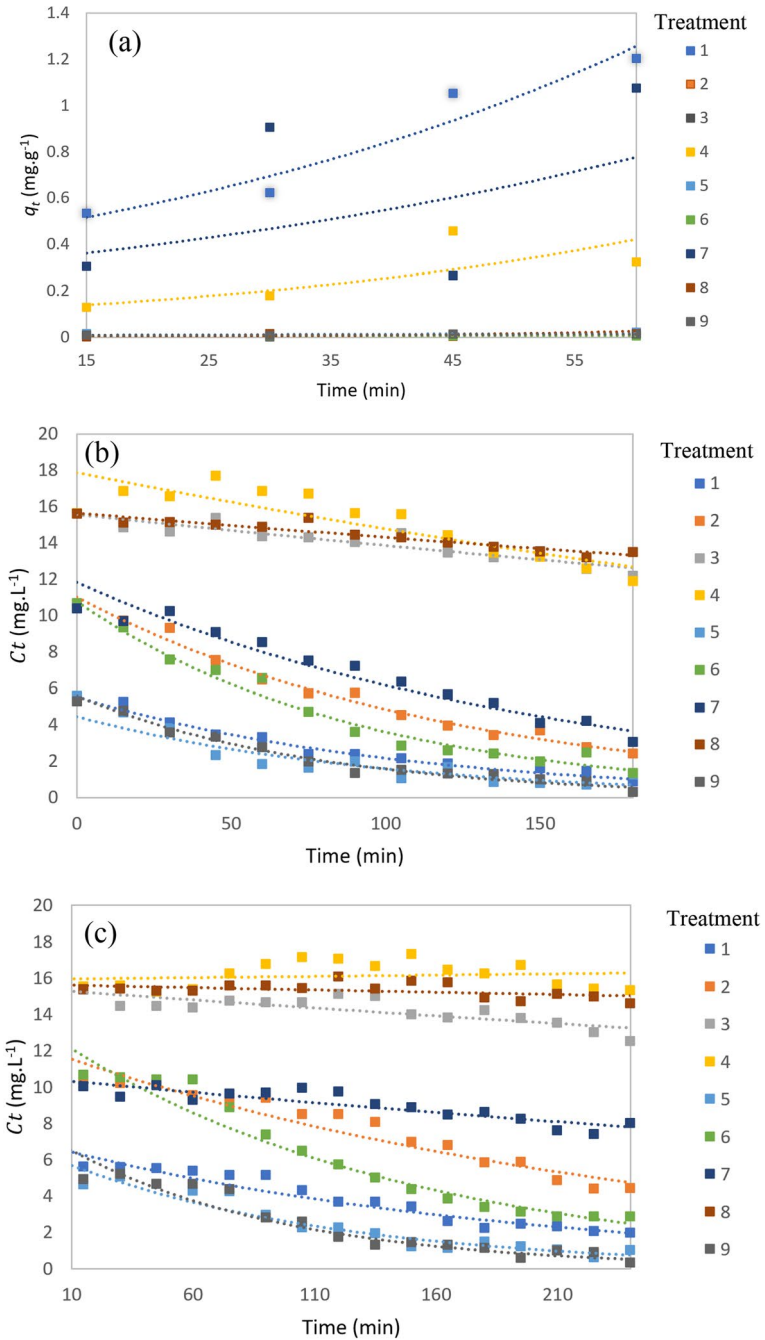


Fig. 4 Kinetic modeling of malathion removal under different processes: **a)** adsorption, **b)** photocatalysis and **c)** adsorption–photocatalysis. The experimental conditions of these processes are shown in Table 1 according to the Taguchi methodology

for adsorption–photocatalysis. These results coincided with the lowest degradation rates obtained in this study, with k values of 0.0009 min^{-1} and 0.0002 min^{-1} for the photocatalysis and adsorption–photocatalysis processes, respectively.

Adsorption isotherms

The Langmuir and Freundlich isotherms describe the adsorption process. The Langmuir adsorption isotherm is a theoretical representation of the mass of malathion adsorbed on a given mass of adsorbent. This isotherm corresponds to a distribution of the pollutant molecules on the surface of the adsorbent material as a monolayer. This means that when the pollutant molecules bind to the active site of the adsorbent, no further adsorption occurs. The Freundlich adsorption isotherm is an empirical representation that considers the multilayer adsorption of the pollutant [5]. The Langmuir and Freundlich isothermal constants were calculated using non-linear least squares fitting to the untransformed original equations according to the methodology proposed by Lente [53]. These constants are shown in Table 5. The value of R^2 close to 1 indicates that the adsorption process was favorable. The results show that the SA polymer better fits the Langmuir isotherm since a higher coefficient of determination value was found ($R^2 = 0.9992$). This result indicates a monolayer adsorption process when using SA polymer in the biopolymer-based photocatalysis process. Under these conditions, malathion is adsorbed uniformly on the superficial layer of the beads of the polymer, limiting the adsorption efficiency. These results are similar to those reported by Han et al. [21] who reported the adsorption of methylene blue by polyacrylonitrile (PAN) beads, coated with polyvinylalcohol (PVA).

The adsorption kinetic study also revealed that the PVP polymer better fitted the Freundlich isotherm with an R^2 value of 0.9519, which indicates a multilayer adsorption process occurs when this polymer is used. These results are similar to those reported by Hosseini et al. [5] who also reported that the adsorption of malathion using a sodium alginate/biosilicate/magnetite (SABM) nanocomposite as adsorbent showed a good fit by Freundlich isotherm ($R^2 = 0.9959$).

In Table 5, it is noteworthy that low R^2 values were obtained for the PVA polymer when fitting experimental data to the Langmuir and Freundlich isotherm equations ($R^2 = 0.0698$ and $R^2 = 0.0105$, respectively). Since the fitting parameters obtained from the isotherm equations were not satisfactory, it can be inferred that a low adsorption strength or affinity was found for the PVA polymer. This situation could be desirable in the biopolymer-based photocatalysis process. Previously, this study

Table 5 Kinetic parameters of the Langmuir and Freundlich adsorption isotherms

Polymer	Langmuir			Freundlich		
	q_{\max} (mg g^{-1})	K_L (L g^{-1})	R^2	K_F	n	R^2
SA	0.046210	455.042476	0.9992	0.0167764	2.4545901	0.989
PVA	0.031031	425.704774	0.0698	3.6450207	− 22.675737	0.0105
PVP	0.096246	43.1084557	0.4745	498.08103	0.8845644	0.9519

evidenced an interference in the photocatalytic activity because of the presence of an adsorbed multilayer on the surface beads, which resulted in a lower degradation efficiency. Since the PVA biopolymer showed a low affinity for malathion, it will be less likely to form unwanted interferences, improving the degradation efficiency with a longer useful life of the polymer. This situation coincides with the results obtained in this study, where treatment 9 (using PVA biopolymer) showed the maximum degradation rate and efficiency in the L9 Taguchi experimental design.

Conclusions

This study proved the feasibility of using polymer beads (SA, PVA, and PVP) to immobilize a catalyst (TiO_2) in a UV oxidation process for malathion removal. The characterization of the beads by Scanning Electron Microscopy demonstrated the presence of malathion on the surface of the polymers. In a biopolymer-based photocatalysis process, the effect of adsorption and photocatalysis were evaluated independently, but also the synergistic effect of adsorption–photocatalysis, by using the removal rate and efficiency. These processes were also compared with the photocatalysis process using TiO_2 nanoparticles in suspension. The TiO_2 supported on the polymer beads (SA/ TiO_2 , PVA/ TiO_2 , PVP/ TiO_2) achieved removal efficiencies of 99% after 180 min of treatment. The best operating conditions were obtained using a Taguchi L9 experimental design. The adsorption process when using SA adjusted to the Langmuir mathematical model, suggesting that a monolayer adsorption process occurs. The adsorption process when using PVP fitted the Freundlich mathematical model, suggesting that a multilayer adsorption process occurs. The statistical analysis showed that the multilayer adsorption interfered with the photocatalysis process since a higher degradation efficiency was observed when the direct photocatalysis was conducted in comparison with the adsorption–photocatalysis process. Therefore, this study suggests carrying out the photocatalysis process without waiting for the beads to adsorb malathion and/or using an adsorbent with low adsorption affinity. The results also demonstrated that the use of catalyst support (TiO_2) increased the efficiency of the photocatalysis process in comparison with the photodegradation of malathion using the catalyst in suspension.

Supplementary Information The online version contains supplementary material available at <https://doi.org/10.1007/s11144-023-02515-8>.

Acknowledgements The authors thank TecNM/Instituto Tecnológico de Culiacán for providing the infrastructure to carry out this work and CONAHCYT for the scholarship provided to the first author.

Funding No funding was received for conducting this study.

Data availability Not applicable

Declarations

Conflict of interest The author declares no competing interests.

Ethical approval Not applicable.

References

1. Raju IM, Rao SKV, Divya G (2019) Poly 3-thenoic acid sensitized, copper doped anatase/brookite TiO₂ nanohybrids for enhanced photocatalytic degradation of an organophosphorus pesticide. *J Environ Chem Eng* 7(4):103211
2. Li W, Zhao Y, Yan X, Duan J, Saint CP, Beecham S (2019) Transformation pathway and toxicity assessment of malathion in aqueous solution during UV photolysis and photocatalysis. *Chemosphere* 234:204–214
3. Rangel-Peraza JG, Prado MAR, Amabilis-Sosa LE, Bustos-Terrones YA, Ramírez-Pereda B (2020) Malathion removal through peroxi-electrocoagulation and photocatalytic treatments optimization by statistical analysis. *Int J Electrochem Sci* 15:8253–8264
4. Vassalini I, Gjipalaj J, Crespi S, Gianoncelli A, Mella M, Ferroni M, Alessandri I (2020) Alginate-derived active blend enhances adsorption and photocatalytic removal of organic pollutants in water. *Adv Sustain Syst* 4(7):1900112
5. Hosseini M, Kamani H, Esrafil A, Badi MY, Gholami M (2019) Removal of malathion by sodium alginate/biosilicate/magnetite nanocomposite as a novel adsorbent: kinetics, isotherms, and thermodynamic. *Study Health Scope* 8(4):11
6. Juang RS, Chen CH (2014) Comparative study on photocatalytic degradation of methomyl and parathion over UV-irradiated TiO₂ particles in aqueous solutions. *J Taiwan Inst Chem Eng* 45(3):989–995
7. Hermosillo-Nevárez JJ, Bustos-Terrones V, Bustos-Terrones YA, Uriarte-Aceves PM, Rangel-Peraza JG (2020) Feasibility study on the use of recycled polymers for Malathion adsorption: isotherms and kinetic modeling. *Materials* 13(8):1824
8. Ullah S, Li Z, Hasan Z, Khan SU, Fahad S (2018) Malathion induced oxidative stress leads to histopathological and biochemical toxicity in the liver of rohu (*Labeo rohita*, Hamilton) at acute concentration. *Ecotoxicol Environ Saf* 161:270–280
9. Flehi-Slim I, Chargui I, Boughattas S, El Mabrouk A, Belaïd-Nouira Y, Neffati F, Najjar MF, Haouas Z, Ben CH (2015) Malathion-induced hepatotoxicity in male Wistar rats: biochemical and histopathological studies. *Environ Sci Pollut Res Int* 22(22):17828–17838
10. Surendra B, Raju BM, Srikanth KN, Choudhary GL, Francis P, Vengalapati M (2020) Synthesis and characterization of Ni doped TiO₂ nanoparticles and its application for the degradation of Malathion. *Mater Today* 26:1091–1095
11. Pérez-Lucas G, El AatikAliste AM, Hernández V, Fenoll J, Navarro S (2022) Reclamation of aqueous waste solutions polluted with pharmaceutical and pesticide residues by biological-photocatalytic (solar) coupling in situ for agricultural reuse. *Chem Eng J* 448:137616
12. Tu H, Li D, Yi Y, Liu R, Wu Y, Dong X, Deng H (2019) Incorporation of rectorite into porous polycaprolactone/TiO₂ nanofibrous mats for enhancing photocatalysis properties towards organic dye pollution. *Compos Commun* 15:58–63
13. Maldonado-Larios L, Mayen-Mondragón R, Martínez-Orozco RD, Páramo-García U, Gallardo-Rivas NV, García-Alamilla R (2020) Electrochemically assisted fabrication of titanium-dioxide/polyaniline nanocomposite films for the electroremediation of Congo red in aqueous effluents. *Synth Met* 268:116464
14. González-González RB, Parra-Saldívar R, Alsanie WF, Iqbal HM (2022) Nanohybrid catalysts with porous structures for environmental remediation through photocatalytic degradation of emerging pollutants. *Environ Res* 214:113955
15. Zhao L, Deng J, Sun P, Liu J, Ji Y, Nakada N, Yang Y (2018) Nanomaterials for treating emerging contaminants in water by adsorption and photocatalysis: systematic review and bibliometric analysis. *Sci Total Environ* 627:1253–1263
16. Reveendran ST (2018) Application of experimental design for dyes removal in aqueous environment by using sodium alginate-TiO₂ thin film. *Chem Data Collect* 15:32–40
17. Ortíz MDJR, Valencia RH, Parra GA, Morales PA (2021) Síntesis verde de materiales nanoestructurados de ZnO en la degradación de contaminantes orgánicos por medio de la fotocatalisis heterogénea. *Rev Cienc Tecnol* 4(4):299–313
18. Mehmood CT, Zhong Z, Zhou H, Xiao Y (2020) Constructing porous beads with modified polysulfone-alginate and TiO₂ as a robust and recyclable photocatalyst for wastewater treatment. *J Water Process Eng* 38:101601


19. Farzadkia M, Esrafilii A, Baghapour MA, Shahamat YD, Okhovat N (2013) Degradation of metronidazole in aqueous solution by nano-ZnO/UV photocatalytic process. *Desalin Water Treat* 52(25–27):4947–4952
20. Rodriguez-Mata AE, Tzompantzi FJ, Amabilis-Sosa LE, Diaz-Peña I, Bustos-Terrones Y, Rangel-Peraza JG (2018) Characterization of $\text{SO}^{2-}_4/\text{ZnO}$ and photo degradation kinetics of 2, 4-Dichlorophenoxyacetic Acid (2, 4-D). *Kinet Catal* 59(6):720–726
21. Han Z, Jin J, Wang Y, Zhang Z, Gu J, Ou M, Xu X (2019) Encapsulating TiO_2 into polyvinyl alcohol coated polyacrylonitrile composite beads for the effective removal of methylene blue. *J Braz Chem Soc* 30:211–223
22. Elbarbary AM, Gad YH (2021) Radiation synthesis and characterization of poly (vinyl alcohol)/acrylamide/ $\text{TiO}_2/\text{SiO}_2$ nanocomposite for removal of metal ion and dye from wastewater. *J Inorg Organomet Polym Mater* 31(10):4103–4125
23. Hui KC, Suhaimi H, Sambudi NS (2021) Electrospun-based TiO_2 nanofibers for organic pollutant photo degradation: a comprehensive review. *Rev Chem Eng* 38(6):641–668
24. Moustafa H, Karmalawi AM, Youssef AM (2021) Development of hybrid TiO_2 nanocomposites coated with dapsone and their effects on UV radiation, mechanical, thermal properties and antibacterial activity of PVA bionanocomposites. *Environ Nanotechnol Monit Manag* 16:100482
25. Kadam AN, Dhabbe RS, Kokate MR, Gaikwad YB, Garadkar KM (2014) Preparation of N doped TiO_2 via microwave-assisted method and its photocatalytic activity for degradation of Malathion. *Spectrochim Acta A* 133:669–676
26. Akter S, Islam MS, Kabir MH, Shaikh MA, Gafur MA (2022) UV/ TiO_2 photo degradation of metronidazole, ciprofloxacin and sulfamethoxazole in aqueous solution: an optimization and kinetic study. *Arab J Chem* 15(7):103900
27. Karkeh-Abadi F, Saber-Samandari S, Saber-Samandari S (2016) The impact of functionalized CNT in the network of sodium alginate-based nanocomposite beads on the removal of Co (II) ions from aqueous solutions. *J Hazard Mater* 312:224–233
28. Nouri L, Hemidouche S, Boudjemaa A, Kaouah F, Sadaoui Z, Bachari K (2020) Elaboration and characterization of photobiocomposite beads, based on titanium (IV) oxide and sodium alginate biopolymer, for basic blue 41 adsorption/photocatalytic degradation. *Int J Biol Macromol* 151:66–84
29. Lee SJ, Lim HW, Park SH (2021) Adsorptive seawater desalination using MOF-incorporated Cu-alginate/PVA beads: ion removal efficiency and durability. *Chemosphere* 268:128797
30. Dalponte I, de Sousa BC, Mathias AL, Jorge RM (2019) Formulation and optimization of a novel TiO_2 /calcium alginate floating photocatalyst. *Int J Biol Macromol* 137:992–1001
31. Gopinath KP, Madhav NV, Krishnan A, Malolan R, Rangarajan G (2020) Present applications of titanium dioxide for the photocatalytic removal of pollutants from water: a review. *J Environ Manag* 270:110906
32. Sakarkar S, Muthukumaran S, Jegatheesan V (2020) Evaluation of polyvinyl alcohol (PVA) loading in the PVA/titanium dioxide (TiO_2) thin film coating on polyvinylidene fluoride (PVDF) membrane for the removal of textile dyes. *Chemosphere* 257:127144
33. Ainali NM, Kalaronis D, Evgenidou E, Bikiaris DN, Lambropoulou DA (2021) Insights into biodegradable polymer-supported titanium dioxide photocatalysts for environmental remediation. *Macromolecules* 1(3):201–233
34. Sherugar P, Naik NS, Padaki M, Nayak V, Gangadharan A, Nadig AR, Déon S (2021) Fabrication of zinc doped aluminum oxide/polysulfone mixed matrix membranes for enhanced antifouling property and heavy metal removal. *Chemosphere* 275:130024
35. Rafaie HA, Shohaimi NA, Ramli NI, Ishak ZI, Rosmi MS, Mohamed MA, Hir ZA (2022) Application of hybrid polymeric materials as photocatalyst in textile wastewater. In: *Polymer technology in dye-containing wastewater*, pp 101–143
36. Balakrishnan A, Appunni S, Chinthala M (2022) Biopolymer-supported TiO_2 as a sustainable photocatalyst for wastewater treatment: a review. *Environ Chem Lett* 20:3071–3098
37. Zanella R (2012) Metodologías para la síntesis de nanopartículas: controlando forma y tamaño Mundo Nano. *Revista Interdisciplinaria en Nanociencias y Nanotecnología* 5(1):69–81
38. Martínez Rojas V, Matejova L, López Milla A, Cruz G, Solís Veliz J, Gómez León M (2015) Obtención de partículas de TiO_2 por sol-gel, asistido con ultrasonido para aplicaciones fotocatalíticas. *Rev Soc Quím Perú* 81:201–211
39. Al Qarni F, Alomair N, Mohamed H (2019) Environment-friendly nanoporous titanium dioxide with enhanced photocatalytic activity. *Catalysts* 9:799

40. Bustos-Terrones YA, Estrada-Vázquez R, Ramírez-Pereda B, Bustos-Terrones V, Rangel-Peraza JG (2020) Kinetics of a fixed bed reactor with immobilized microorganisms for the removal of organic matter and phosphorous. *Water Environ Res* 92(11):1956–1965
41. Basu H, Pimple MV, Saha S, Patel A, Dansena C, Singhal RK (2020) TiO₂ microsphere impregnated alginate: a novel hybrid sorbent for uranium removal from aquatic bodies. *New J Chem* 44(10):3950–3960
42. Rancic SM, Nikolic-Mandic SD, Mandic LM (2005) Kinetic spectrophotometric method for gold(III) determination. *Anal Chim Acta* 547(1):144–149
43. Fazal T, Razzaq A, Javed F, Hafeez A, Rashid N, Amjad US, Rehman F (2020) Integrating adsorption and photocatalysis: a cost effective strategy for textile wastewater treatment using hybrid biochar-TiO₂ composite. *J Hazard Mater* 390:121623
44. Chakhtouna H, Zari N, Bouhfid R, Qaiss A, Benzeid H (2021) Novel photocatalyst based on date palm fibers for efficient dyes removal. *J Water Process Eng* 43:102167
45. Sarkar S, Chakraborty S, Bhattacharjee C (2015) Photocatalytic degradation of pharmaceutical wastes by alginate supported TiO₂ nanoparticles in packed bed photo reactor (PBPR). *Ecotoxil Environ Saf* 121:263–270
46. Chen JH, Liu QL, Hu SR, Ni JC, He YS (2011) Adsorption mechanism of Cu (II) ions from aqueous solution by glutaraldehyde crosslinked humic acid-immobilized sodium alginate porous membrane adsorbent. *Chem Eng J* 173(2):511–519
47. Bolboacă SD, Jäntschi L (2007) Design of experiments: useful orthogonal arrays for number of experiments from 4 to 16. *Entropy* 9(4):198–232
48. Suresh R, Rajendran S, Hoang TKA, Vo D-VN, Siddiqui MN, Cornejo-Ponce L (2021) Recent progress in green and biopolymer based photocatalysts for the abatement of aquatic pollutants. *Environ Res* 199:111324
49. Arikal D, Kallingal A (2021) Photocatalytic degradation of azo and anthraquinone dye using TiO₂/MgO nanocomposite immobilized chitosan hydrogels. *Environ Technol* 42(15):2278–2291
50. Kumar R, George L, Jun Z, Mukherji S (2022) Photocatalytic activity of graphene oxide-TiO₂ nanocomposite on dichlorvos and Malathion and assessment of toxicity changes due to photo degradation. *Chemosphere* 308:136402
51. Kralj MB, Cernigoj U, Franko M, Trebse P (2007) Comparison of photocatalysis and photolysis of Malathion, isoMalathion, malaoxon, and commercial Malathion—products and toxicity studies. *Water Res* 41:4504–4514
52. Yu H, Wang X, Sun H, Huo M (2010) Photocatalytic degradation of malathion in aqueous solution using an Au–Pd–TiO₂ nanotube film Au–Pd–TiO₂. *J Hazard Mater* 184(1–3):753–758
53. Lente G (2015) Deterministic kinetics in chemistry and systems biology: the dynamics of complex reaction networks. Springer, New York
54. Fernández JA, Cardozo MG, Carrascal AK, Salcedo JC, Pedroza AM, Daza CE (2015) Tratamiento de agua residual de microbiología usando películas delgadas de TiO₂. *Ingeniería Y Competitividad* 17(1):35–48
55. Alrousan DM, Dunlop PS, McMurray TA, Byrne JA (2009) Photocatalytic inactivation of *E. coli* in surface water using immobilised nanoparticle TiO₂ films. *Water Res* 43(1):47–54
56. Athanasekou C, Romanos GE, Papageorgiou SK, Manolis GK, Katsaros F, Falaras P (2017) Degradación fotocatalítica de contaminantes emergentes de cromo hexavalente a través de nanoestructuras de dióxido de titanio avanzadas. *Revista de ingeniería química* 318:171–180

Publisher's Note Springer Nature remains neutral with regard to jurisdictional claims in published maps and institutional affiliations.

Springer Nature or its licensor (e.g. a society or other partner) holds exclusive rights to this article under a publishing agreement with the author(s) or other rightsholder(s); author self-archiving of the accepted manuscript version of this article is solely governed by the terms of such publishing agreement and applicable law.

Authors and Affiliations

Rogelio Estrada-Vázquez¹ · Mabel Vaca-Mier² · Victoria Bustos-Terrones³ · Jesús Gabriel Rangel-Peraza¹ · Juan G. Loaiza¹ · Jhonatan J. Hermosillo-Nevárez⁴ · Yaneth A. Bustos-Terrones⁵ 

✉ Yaneth A. Bustos-Terrones
yaneth.bt@culiacan.tecnm.mx

¹ División de Estudios de Posgrado e Investigación, TecNM-Instituto Tecnológico de Culiacán, Juan de Dios Bátiz, No. 310. Col. Guadalupe, 80220 Culiacán, Sinaloa, Mexico

² Universidad Autónoma Metropolitana, Ciencias Básicas e Ingeniería, San Pablo, No. 180. Col. Reynosa Tamaulipas, Azcapotzalco, 02200 Ciudad de Mexico, CDMX, Mexico

³ Dirección Académica de Ingeniería en Tecnología Ambiental, Universidad Politécnica del Estado de Morelos, Boulevard Cuauhnáhuac, No. 556. Col. Lomas del Texcal, 62550 Jiutepec, Morelos, Mexico

⁴ Boulevard Lola Beltrán y Boulevard Rolando Arjona, Universidad Autónoma de Occidente-Unidad Regional Culiacán, Col. 4 de Marzo, 80020 Culiacán, Sinaloa, Mexico

⁵ División de Estudios de Posgrado e Investigación, CONAHCYT-TecNM-Instituto Tecnológico de Culiacán, Juan de Dios Bátiz, No. 310. Col. Guadalupe, 80220 Culiacán, Sinaloa, Mexico